Research article

Journal of RAMAN SPECTROSCOPY

Received: 30 September 2013 Revised: 6 December 2013 Accepted: 7 December 2013 Published online in Wiley Online Library: 16 January 2014

(wileyonlinelibrary.com) DOI 10.1002/jrs.4440

A non-destructive approach for doping profiles characterization by micro-Raman spectroscopy: the case of B-implanted Ge

A. Sanson,[a]* E. Napolitani,[a] A. Carnera,[a] G. Impellizzeri,[b] M. Giarola[c] and G. Mariotto[c]

B-implanted Ge samples have been investigated by micro-Raman spectroscopy under different excitation wavelengths, with the aim of gaining insights about the B distribution at different depths beneath the sample surface. The intensities, observed under the different excitation wavelengths, of the B–Ge Raman peak at about 545 cm^{-1}, which is due to the local vibrational mode of the substitutional B atoms in the Ge matrix, have been used to calibrate the optical absorption lengths in B-implanted Ge. Then, by using these calibrated values, a very sharp correlation between the spectral features of the Ge–Ge Raman peak at ~300 cm^{-1} and the content of substitutional B atoms has been derived. Accordingly, a non-destructive approach, based on micro-Raman spectroscopy under different excitation wavelengths, is presented to estimate, at least at the lowest depths, the carrier concentration profiles from the spectral features of the Ge–Ge Raman peak. Copyright © 2014 John Wiley & Sons, Ltd.

Keywords: carrier concentration profiles; substitutional atoms; Ge doping; B-implants Ge

Introduction

The studies of dopant diffusion and electrical activation processes are of primary importance for the evolution of semiconductor devices.[1] In this regard, spreading resistance profiling (SRP) analysis is very important because it allows determining from resistivity measurements the carrier concentration profile, i.e. the concentration profile of substitutional dopant atoms.[2] Unfortunately, in the sample preparation, SRP requires a beveling procedure that makes this technique complex and, above all, destructive.

Micro-Raman spectroscopy is widely used in the study of the physical and chemical properties of semiconductors at the micro or sub-micro scale. For example, it is currently exploited for determining the crystallinity degree and the local crystal orientation of thin films and nano-structures, for strain characterizations, and for local temperature detection in devices under operation.[3–5] In the last years, micro-Raman spectroscopy has also been tentatively used in the study of doping profiles in crystalline semiconductors. O'Reilly *et al*. reported,[6] for Sb-implanted Si, a correlation between Si Raman peak shift and peak carrier concentration measured by differential Hall technique. By combining micro-Raman spectroscopy with small-angle beveling preparation techniques, Becker *et al*.[7] found, in the framework of Fano resonance theory, a rough linear relationship between the free hole concentration and the reciprocal of the symmetry parameter of Si Raman peak. Shortly after, Perova and coworkers,[8,9] studying the structural damage in Ge wafers implanted with H and He, obtained a correlation between Raman mapping measurements on beveled samples and SRP analyses. Similar studies were performed by Srnanek *et al*.[10,11] on doped GaAs-based beveled structures. Most recently, we estimated the electrically active dopant profiles in Al-implanted Ge still by combining micro-Raman spectroscopy with small-angle beveling technique.[12]

These works suggest that micro-Raman spectroscopy could provide a suitable approach, complementary to SRP, for dopant profile characterizations in crystalline semiconductors. Nevertheless, this technique is not currently employed for these purposes because it is not yet refined for quantitative characterizations and, above all, because when combined with the beveling method, it is destructive too, thus resulting not really advantageous with respect to the SRP technique.

An alternative and non-destructive method to estimate the carrier concentration profiles in Ge-implanted samples consists in carrying out micro-Raman spectroscopy measurements under excitation of different laser wavelengths. In fact, in the visible region, crystalline Ge has an optical absorption length much lower than that of crystalline Si, ranging from about 10 to about 150 nm.[13] Therefore, by using different excitation wavelengths, we can study the vibrational dynamics of Ge-implanted samples at different depths beneath the sample surface, avoiding to bevel it. This non-destructive approach, combined with a reverse Monte Carlo fitting procedure, was recently exploited by us to estimate the carrier concentration profiles in Al-implanted Ge samples.[14] In this work, we aim to apply a similar procedure in

* *Correspondence to: Andrea Sanson, Dipartimento di Fisica e Astronomia 'Galileo Galilei', Università di Padova, Via Marzolo 8, I-35131 Padova, Italy. E-mail: andrea.sanson@unipd.it*

a *CNR-IMM MATIS and Dipartimento di Fisica e Astronomia 'G. Galilei', Universitμa di Padova, Via Marzolo 8, I-35131 Padova, Italy*

b *CNR-IMM MATIS at Dipartimento di Fisica e Astronomia, Universitμa di Catania, Via S. So¯a 64, I-95123 Catania, Italy*

c *Dipartimento di Informatica, Universitμa di Verona, Strada le Grazie 15, I-37134 Verona, Italy*

B-implanted Ge samples to check and, in the meanwhile, to improve our method. Moreover, it should be pointed out that the technological interest for B-doped Ge is actually stronger that for Al-doped Ge, so that our present manuscript might match even more relevant interest within the related scientific community.

Experimental

Ge Czochralski wafers, (100)-oriented, *n*-type (Sb-doped with a resistivity higher than 40 Ωcm, i.e. $<10^{14}$ Sb/cm^3) were implanted at liquid nitrogen temperature with B ions at 35 KeV at different fluences: 2.8×10^{15} B/cm^2 (low fluence) and 7.6×10^{15} B/cm^2 (high fluence) and then annealed at 360 °C for 1 h in N_2 atm to induce a complete regrowth of the Ge matrix by solid-phase epitaxy and a very high incorporation of B in substitutional sites (~100% of the implanted B). Consequently, the carrier concentration profiles of our samples have been derived from the combination of Hall measurements and strain profiles obtained by high-resolution X-ray diffraction.[15,16] We would point out that to prepare B-implanted Ge samples with these properties is far from trivial. Anyhow, the number of samples here prepared is sufficient to validate the reliability of our method, also thanks to the large number of laser excitation wavelengths used in the succeeding text.

Room-temperature polarized micro-Raman measurements were carried out in the usual backscattering geometry by means of a triple monochromator (Horiba-Jobin Yvon, model T64000), equipped with holographic gratings having 1800 lines/mm, and set in double subtractive/single configuration. After the filtering by the fore double monochromator, the scattered radiation was detected at the spectrometer output by a multichannel charge-coupled-device detector, with 1024 × 256 pixels, cooled by liquid nitrogen. The spectra were excited by the 488.0, 514.5, 568.2, and 647.1 nm line of a mixed Ar–Kr gas laser and by the 632.8 nm line of a mixed He–Ne gas laser. The laser beams were focused onto a spot of ~2 μm in size through the lens of a 100× microscope objective with numerical aperture N.A. = 0.90. To avoid thermal heating, the laser power on the sample surface was kept well below 15 mW (depending on the laser wavelength). The spectral resolution was, for all the excitation wavelengths, better than 0.6 cm^{-1}/pixel. All the spectra were calibrated in wavenumber using some emission lines of a Ne spectral lamp assumed as reference. In order to maximize the intensity of both B–Ge and Ge–Ge Raman peaks, all the Raman spectra were recorded in crossed XY polarization (X and Y electric field directions, respectively, of incident and scattered light) aligning the X-direction along the [100] crystallographic axis of the sample (for more details, see the study of Sanson *et al.*[17]). For each laser excitation line, repeated micro-Raman measurements were performed from different regions of the sample surface, and the spectra showed a very good reproducibility.

Results and discussion

B–Ge Raman peak and optical absorption length calibration

Selected Raman spectra from our B-implanted Ge samples, carried out in crossed polarization under excitation by three different laser lines, are shown in Fig. 1. The corresponding Raman spectra of pure Ge wafer are also reported for comparison.

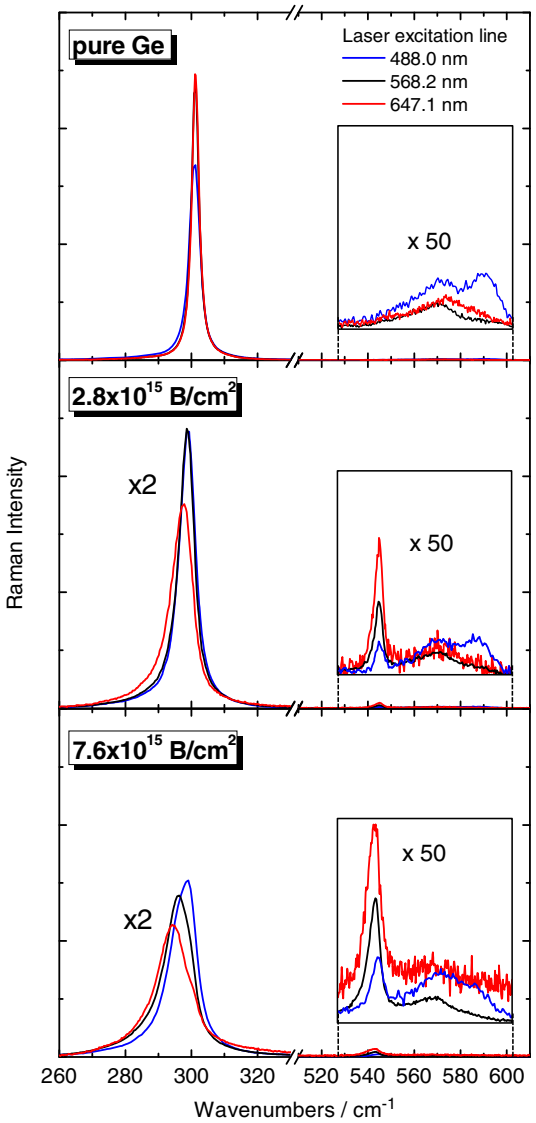

Figure 1. Raman spectra in pure Ge (top panel), here used as reference, and in B-implanted Ge samples with fluence of 2.8×10^{15} B/cm^2 (middle panel) and 7.6×10^{15} B/cm^2 (bottom panel) recorded under excitation laser line 488.0, 568.2, and 647.1 nm (blue, black, and red solid lines, respectively). The vertical scale in the middle and bottom panels is magnified two times to show the Ge–Ge peak at ~300 cm^{-1}. In the insets, the vertical scale is magnified 50 times to show the B–Ge Raman peak at ~545 cm^{-1}. The band between 540 and 600 cm^{-1} is due to the second-order Raman spectrum of Ge.[18] The spectra are normalized to the area of the Ge–Ge peak at ~300 cm^{-1}. This figure is available in colour online at wileyonlinelibrary.com/journal/jrs

The Raman spectra show a very intense peak at about 300 cm^{-1}, due to the scattering from the expected optical phonon-modes of germanium with F_{2g} symmetry, and a much weaker peak at ~545 cm^{-1}, whose intensity changes with the B ions fluence and laser wavelength. Similarly to our previous Raman studies in Al-implanted Ge,[12,14] this last peak can be assigned to the local vibrational mode of B atoms in substitutional sites. In fact, using the simplified mass-defect secular equation,[19,20] the wavenumber of the vibrational local mode of a substitutional B atom in Ge is estimated to be ~520 cm^{-1}, therefore, taking into account that this simple model assumes that the force constants are the same for the B–Ge and Ge–Ge pairs, close to our experimental wavenumber. Moreover, we have

Journal of RAMAN SPECTROSCOPY

checked, by proper polarized micro-Raman measurements, that the Raman peak at ~545 cm^{-1} obeys the same polarization selection rules as the Ge–Ge peak at ~300 cm^{-1}. Then, because the local symmetry is preserved, we can definitively conclude that the peak at ~545 cm^{-1} is directly related to the local vibrational mode of substitutional B atoms. This conclusion is supported by the recent work of Fukata *et al.*, where the Raman peak observed at ~544 cm^{-1} was assigned to the B local vibrations in Ge nanowires.[21]

On the basis of this last finding, with $P_B(x)$ indicating the concentration of substitutional B atoms (B/cm^3) at depth x beneath the sample surface, the integrated intensity of the B–Ge Raman peak at ~545 cm^{-1} given at the laser wavelength λ_i should be proportional to the integral

$$I(\lambda_i) = \int_0^{\infty} P_B(x) exp[-2x/L(\lambda_i)]dx \qquad (1)$$

where $L(\lambda_i)$ indicates the corresponding optical absorption length,* and the term $exp[-2x/L(\lambda_i)]$ takes account of the optical absorption of both incident and scattered light.† In a first step, we have used for $L(\lambda_i)$ the values calculated by using the absorption coefficient α reported in the study of Aspnes and Studna[13] for pure Ge, listed in the column (a) of Table 1. Hence, for each sample and laser wavelength, the integral (1) has been calculated taking, as $P_B(x)$ distribution, the substitutional B concentration profiles determined from the strain profiles reported in the study of Bisognin *et al.*[15] Afterwards, the integrated intensity of the B–Ge Raman peak, evaluated as the area of the peak at ~545 cm^{-1} (after subtracting straight line between ~530 and 555 cm^{-1}) normalized to the area of the nearby Ge–Ge Raman peak, has been plotted against the values for the integral (1), as displayed in the top panel Fig. 2.

Contrary to what expected, this figure shows a deviation of the calculated values from the linear behavior. Because this deviation is very similar in the two samples, we can infer that it might be due to the wrong values assigned for $L(\lambda_i)$. Accordingly, for each laser wavelength, the values of $L(\lambda_i)$ have been calibrated in order to obtain a linear relationship between B–Ge Raman peak intensity and integral (1), as it is shown in the bottom panel of Fig. 2. In the following of this paper, these calibrated values for $L(\lambda_i)$, listed in column (b) of Table 1, will be used for the analysis of the Ge–Ge Raman peak and in the subsequent reconstruction of the B-doping profiles. The same values could also be adopted for any type of B implantation in Ge. We would point out that the regular trend obtained for the Ge–Ge Raman peak in the following section (Fig. 3) validates the soundness of the $L(\lambda_i)$ calibration here performed.

Table 1. Optical absorption length $L(\lambda_i)$ (in nm) calculated by using the absorption coefficient α given in the study of Aspnes and Studna[13] for pure Ge (column a) and calibrated in this work for B-implanted Ge (column (b))

λ_i	$L(\lambda_i)$ (a)	$L(\lambda_i)$ (b)
488.0	16.5	22.4
514.5	17.2	26.0
568.2	25.2	43.7
632.8	72.6	64.9
647.1	85.0	66.5

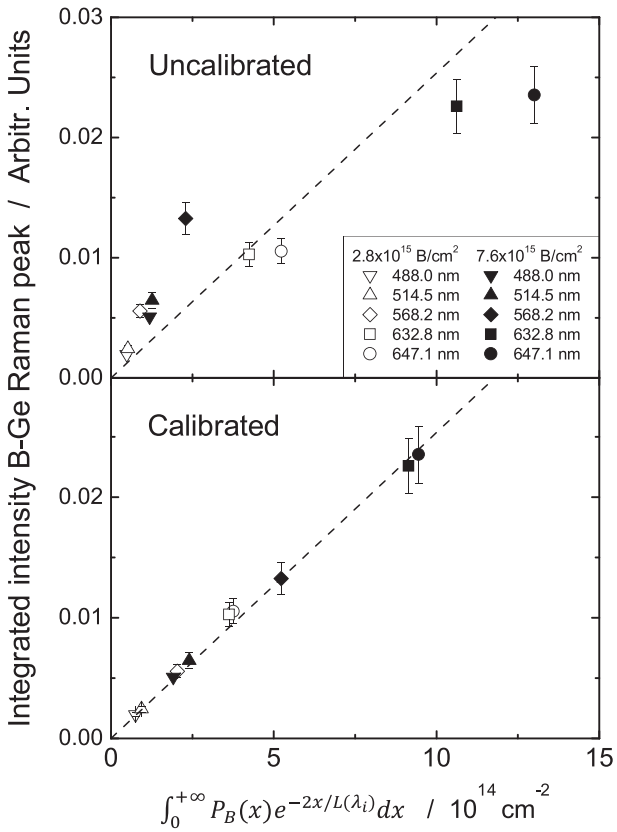

Figure 2. Intensity of the B–Ge Raman peak plotted *versus* the density of substitutional B atoms probed by Raman, estimated by the strain profiles given in the study of Bisognin *et al.*[15] and using the optical absorption length $L(\lambda_i)$ *a*) calculated by using the absorption coefficient α reported in the study of Aspnes and Studna[13] for pure Ge (top panel) *b*) calibrated in this work for B-implanted Ge (bottom panel).

Ge–Ge Raman peak and doping profile simulation

After the calibration of the optical absorption length by the intensity of the B–Ge Raman peak, we now focus on the Ge–Ge Raman band peaked at ~300 cm^{-1}.

Figure 3 shows its average position, full width at half maximum (FWHM), and skew parameter (which measures the peak asymmetry), all calculated‡ compared with the Raman spectra of pure Ge recorded under the same excitation wavelength, plotted as a function of integral (1). This integral was calculated, for each sample and excitation wavelength, using as $P_B(x)$ distribution the corresponding concentration profile of substitutional B atoms derived from Bisognin *et al.*[15]

*With the term 'optical absorption length', we refer here to the inverse of the absorption coefficient α (see Aspnes and Studna[13]), i.e., $L(\lambda_i) = 1/\alpha(\lambda_i)$ is the depth in which the light intensity at the wavelength λ_i is attenuated by a factor 1/e.

†We specify that L is an 'effective value': with L_i and L_s indicating, respectively, the optical absorption length of the incident and scattered light (i.e., Stokes shifted Raman scattering at ~545 cm^{-1}), the exponential term in Eq. 1 is $exp[-x/L_i] \cdot exp[-x/L_s] = exp[-2x/L]$, where $L = 2L_iL_s/(L_i + L_s)$

‡In the calculation of the average position, FWHM, and skew parameter, with respect to pure Ge, it is important to maintain the same spectral range for pure Ge and B-implanted samples (in the present case, 260–340 cm^{-1})

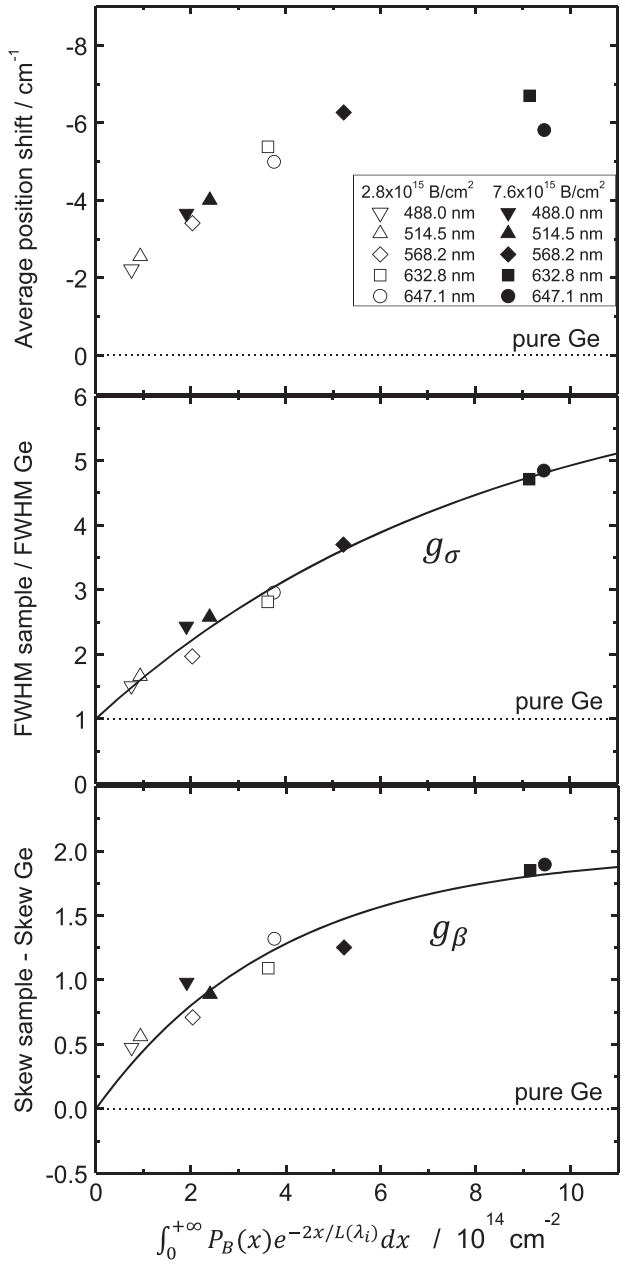

Figure 3. Average position, full width at half maximum and skew parameter (top, middle, and bottom panels, respectively) of the Ge–Ge Raman peak at ~300 cm^{-1} in B-implanted Ge samples, calculated with respect to pure Ge and plotted against the density of substitutional B atoms probed by Raman, which has been estimated by the strain profiles given in the study of Bisognin *et al.*[15] and by using the calibrated optical absorption length L (λ_i) for B-implanted Ge listed in the column (b) of Table 1. The solid lines are the average functions used in the fitting procedure (see text).

The figure reveals the presence of a sharp correlation between the spectral features of the Ge–Ge Raman peak and the content of substitutional B atoms, directly related to the amount of electrically active carriers. On the other hand, it is well known that for high doping levels, the first-order Raman spectra can be heavily affected by the carrier concentration.[22] Other possible effects, either due to phonon confinement or to the presence of strain, can be neglected in the present case. In fact, in our implanted samples, Ge nanocrystalline domains or cluster formation can be ruled out, whereas the lattice strain, whose maximum value does not exceed ~0.17%,[15] gives a Raman peak shift largely lower than 1 cm^{-1}, i.e. negligible.[23] Therefore, the regular change in shape of the Ge–Ge Raman peak evident from Fig. 3 can be exploited to obtain information on the carrier concentration profiles.

To this aim, the experimental data shown in the middle and bottom panel of Fig. 3 were fitted to obtain the average functions for the FWHM and skew parameter, labeled as g_σ and g_β, respectively (solid lines in Fig. 3). Such as in the case of Al-implanted Ge,[14] the average peak position is not here considered because it could be more affected by uncertainties (typically ~1 cm^{-1}) because of the spectra alignment. Afterward, for each laser excitation wavelengths λ_i (in this work is $i = 1,..,5$), we have calculated the integral (1) starting from an arbitrary (flat) $P_B(x)$ distribution. Therefore, the quantities $g_\sigma[I(\lambda_i)]$ and $g_\beta[I(\lambda_i)]$ [($I(\lambda_i)$ is defined in Eqn 1)] are an estimation of the FWHM and skew parameter of the Ge–Ge Raman peak, respectively, for the given $P_B(x)$ distribution probed with the *i*-th laser line. Then, by using a Monte Carlo fitting procedure, $P_B(x)$ is randomly varied to optimize, for each laser wavelength, the match between the estimated and the experimental values for both FWHM and skew parameter, i.e. to minimize the quantity:

$$\sum_{i=1}^{5} |g_\sigma[I(\lambda_i)] - \sigma_i| + |g_\beta[I(\lambda_i)] - \beta_i| \qquad (2)$$

where σ_i and β_i are, respectively, the experimental FWHM and skew parameter measured with the *i*-th laser line.

It is important to highlight that, in the fitting procedure, the $P_B(x)$ distribution must be limited to a finite interval [0, d_{max}], where d_{max} is the maximum depth from which the Raman signal is still significant. The final result for $P_B(x)$ can be influenced from the imposed value of d_{max}. Indeed, if d_{max} is too large, $P_B(x)$ can be wrong at the greatest depths (i.e. where the outgoing Raman signal is negligible), and, as a consequence, $P_B(x)$ is adversely affected at lower depths. On the contrary, if d_{max} is too small, the final $P_B(x)$ is overestimated to compensate the Raman signal coming from the deeper layers now omitted. Therefore, a reliable estimation of d_{max} is important to obtain a reliable $P_B(x)$ distribution. This was made as follows.

A series of fits were performed for different values of d_{max} using a flat $P_B(x)$ distribution, i.e. $P_B(x) = C$ for $x \in [0, d_{max}]$ and 0 otherwise. From Fig. 4, it can be observed that the dependence on d_{max} of

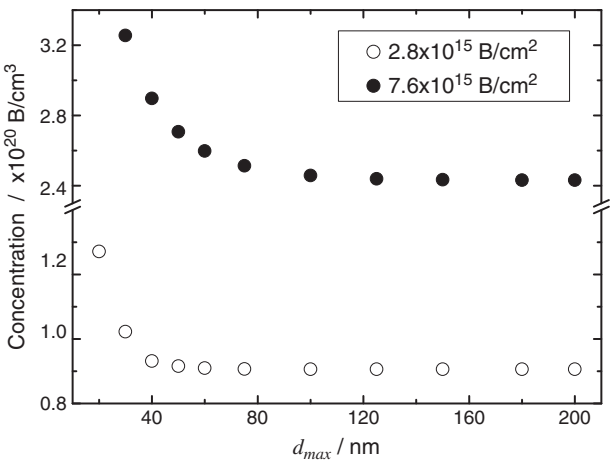

Figure 4. *C* concentration obtained with a flat $P_B(x)$ distribution in low and high dose samples (open and solid circles, respectively), plotted as a function of d_{max} (see text).

Journal of RAMAN SPECTROSCOPY

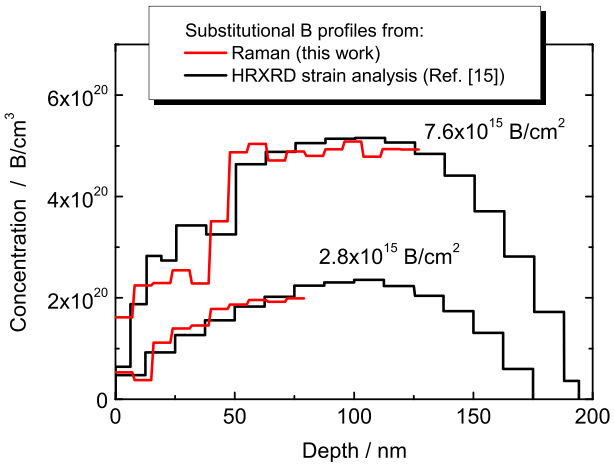

Figure 5. B-doping profiles obtained from strain profiles of Bisognin *et al.*[15] (black lines) and simulated profiles obtained in this work from the Ge–Ge Raman peak (red lines). This figure is available in colour online at wileyonlinelibrary.com/journal/jrs

the resulting concentration C can be neglected above ~80 nm for the low dose sample and above ~130 nm for the high dose sample. Hence, no significant Raman signal is coming out beyond these depths, and, accordingly, we assume such limits for d_{max} in the $P_B(x)$ reconstruction.

Figure 5 displays the simulated $P_B(x)$ profiles obtained in both samples here investigated. It can be observed that the carrier profiles reconstructed from Raman spectroscopy agree very well with the concentration profiles obtained from the strain analysis of Bisognin *et al.*,[15] at least up to the values of d_{max} derived earlier, corresponding to about one to two times the (longest) optical penetration length of the laser line at 647.1 nm.

On the basis of this striking agreement reported in Fig. 5, we can conclude that micro-Raman spectroscopy under different laser wavelengths could be reliably employed to determine the carrier concentration profiles in Ge, i.e. the concentration profiles of substitutional dopants, at least within the range of the maximum optical absorption length and for doping concentrations of the order of ~10^{20} cm^{-3}.

Conclusions

In this paper, B-implanted Ge samples have been studied by micro-Raman spectroscopy under various excitation wavelengths, in order to exploit their different optical penetration depths. In this way, the vibrational dynamics of our implanted Ge samples have been investigated at different depths beneath the sample surface.

By exploiting the intensity of the B–Ge Raman peak at ~545 cm^{-1}, directly related to the content of substitutional B atoms, the optical absorption lengths have been calibrated for B-implanted Ge. By using these calibrated values, a sharp correlation between the spectral features of the Ge–Ge Raman peak at ~300 cm^{-1} and the content of substitutional B atoms has been observed. Hence, starting from the spectral features of the Ge–Ge Raman peak, a non-destructive approach is shown to determine the concentration profiles of substitutional B dopants, namely, the carrier concentration profiles.

Further studies are mandatory to improve the reliability of the method presented. Nevertheless, this work confirms that micro-Raman spectroscopy, under different excitation wavelengths, can be employed as a non-destructive technique for quantitative characterizations of dopant profiles in Ge.

References

[1] L. J. Van der Pauw, *Philips Res. Rep.* **1958**, *13*, 1.
[2] W. Vandervorst, T. Clarysse, P. Eyben, *J. Vac. Sci. Technol. B* **2002**, *20*, 451.
[3] G. Abstreiter, *Appl. Surf. Sci.* **1991**, *50*, 73.
[4] R. Ostermeir, W. Schottky, K. Brunner, G. Abstreiter, W. Weber, *IEEE Trans. Electron Devices* **1992**, *39*, 858.
[5] I. De Wolf, *Semicond. Sci. Tech.* **1996**, *11*, 139.
[6] L. O'Reilly, K. Horan, P. J. McNally, N. S. Bennett, N. E. B. Cowern, A. Lankinen, B. J. Sealy, R. M. Gwilliam, T. C. Q. Noakes, P. Bailey, *Appl. Phys. Lett.* **2008**, *92*, 233506.
[7] M. Becker, U. Gösele, A. Hofmann, S. Christiansen, *J. Appl. Phys.* **2009**, *106*, 074515.
[8] T. S. Perova, B. M. Armstrong, J. Wasyluk, P. Baine, P. Rainey, S. J. N. Mitchell, D. W. McNeill, H. S. Gamble, R. Hurley, *Solid St. Phenom.* **2011**, *178–179*, 295.
[9] J. Wasyluk, P. V. Rainey, T. S. Perova, S. J. N. Mitchell, D. W. McNeill, H. S. Gamble, B. M. Armstrong, R. Hurley, *J. Raman Spectr.* **2011**, *43*, 448.
[10] R. Srnanek, G. Irmer, D. Donoval, A. Vincze, B. Sciana, D. Radziewicz, M. Tlaczala, *Microelectr. J.* **2008**, *39*, 1439.
[11] R. Srnanek, J. Geurts, M. Lentze, G. Irmer, J. Kovac, D. Donoval, D. S. McPhail, P. Kordos, M. Florovic, A. Vincze, B. Sciana, D. Radziewicz, M. Tlaczala, *Thin Sol. Films* **2006**, *497*, 7.
[12] A. Sanson, E. Napolitani, M. Giarola, G. Impellizzeri, V. Privitera, G. Mariotto, A. Carnera, *Apply. Phys. Express* **2013**, *6*, 042404.
[13] D. E. Aspnes, A. A. Studna, *Phys. Rev. B* **1983**; *27*, 985.
[14] A. Sanson, M. Giarola, E. Napolitani, G. Impellizzeri, V. Privitera, A. Carnera, G. Mariotto, *J. Raman Spectr.* **2013**, *44*, 665.
[15] G. Bisognin, S. Vangelista, M. Berti, G. Impellizzeri, M. G. Grimaldi, *J. Appl. Phys.* **2010**, *107*, 103512.
[16] G. Impellizzeri, S. Mirabella, E. Bruno, A. M. Piro, M. G. Grimaldi, *J. Appl. Phys.* **2009**, *105*, 063533.
[17] A. Sanson, E. Napolitani, G. Impellizzeri, M. Giarola, D. De Salvador, V. Privitera, F. Priolo, G. Mariotto, A. Carnera, *Thin Solid Films* **2013**, *541*, 76.
[18] B. A. Weinstein, M. Cardona, *Phys. Rev. B* **1973**, *7*, 2545.
[19] G. Contreras, M. Cardona, A. Compaan, *Solid St. Comm.* **1985**, *53*, 857.
[20] M. A. Renucci, J. B. Renucci, M. Cardona, Light Scattering in Solids (Ed.:Balkanski), Flammarion, Paris, **1971**, p. 326.
[21] N. Fukata, K. Sato, M. Mitome, Y. Bando, T. Sekiguchi, M. Kirkham, J. Hong, Z. L. Wang, R. L. Snyder, *ACS Nano* **2010**, *4*, 3807.
[22] F. Cerdeira, M. Cardona, *Phys. Rev. B* **1972**, *5*, 1440.
[23] C. Y. Peng, C. F. Huang, Y. C. Fu, Y. H. Yang, C. Y. Lai, S. T. Chang, C. W. Liu, *J. Appl. Phys.* **2009**, *105*, 083537.

